ChemComm

Multifunctional Anode with P-Doped Si Nanoparticles in Stress-Buffering Network of Poly-γ-glutamate and Graphene

Journal:	*ChemComm*
Manuscript ID	CC-COM-10-2020-006623
Article Type:	Communication

COMMUNICATION

Multifunctional Anode with P-Doped Si Nanoparticles in Stress-Buffering Network of Poly-γ-glutamate and Graphene

Received 00th January 20xx,
Accepted 00th January 20xx

DOI: 10.1039/x0xx00000x

Ren Na,[a,b] Nadine Madiou [a], Ning Kang[a], Shan Yan[a], Jin Luo[a], Guojun Liu[c], Zhongqiang Shan[b], Jianhua Tian*[b], and Chuan-Jian Zhong*[a]

Here, a new strategy is reported for the preparation of a new class of nanocomposite anode materials consisting of ppm-level phosphorus-doped Si nanoparticles (P-Si) wrapped in a network of poly-γ-glutamate and graphene. The network produces not only a conductivity-enhanced conduit but also a mechanical stress buffer. The incorporation of poly-γ-glutamate in the nanocomposite enables self-healing capability and maintain the electrode structure integrity. This multifunctionality has significant implications for advancing the design of stable Si-based nanomaterials as high-performance anode in Li-ion batteries.

While the invention and commercialization of lithium-ion batteries (LIBs) have changed the world[1], there has been increasing need to improve the limited charge capacity and cycle life of LIBs to meet the ever-growing demand of the energy storage market. In an effort of pursuing higher energy and power density, the exploration of advanced electrode materials with high capacity and long cycle life has been focus of the research frontier.[2] Silicon (Si) is one of the most promising candidates for anode of LIB due to its high capacity, which is almost 10 times of the current commercial graphite. However, the huge volume expansion of Si during cycling processes leads to pulverization of the electrode and subsequent rapid capacity decay, which largely hindered its practical application. The intrinsic low conductivity of Si also affects the rate capability.[3] Progress has been made in addressing these problems, including synthesizing nano-sized Si and preparing composite to enhance the conductivity.[4, 5] Recently, modifying active structure by doping heteroatom has been demonstrated to be an effective way of enhancing the electrochemical property of the anode materials during cycling.[6-8] Computational modeling also reveals that by introducing heteroatoms whose atom radii are smaller than Si atom would cause the shrinkage of crystal structure, thus increasing lithium insertion energy.[9, 10] It is also shown that introducing P atom into Si can control the phase transition during charge/discharge processes.[11] In addition to semiconducting properties, the thermal and chemical stabilities of P-doped Si are also excellent. While the volume change of Si is controlled to some extent, bare P-Si suffers from the capacity decay problem due to instability of the solid-state electrolyte interface (SEI) caused by the repeated volume changes, and the poor coulombic efficiency. Thus, constructing a protecting layer outside P-Si from side reaction with electrolyte has been considered. In previous work, Huang et al. reported micro-sized P-Si/graphite delivered 883 $mAhg^{-1}$ after 200 cycles under a current density of 200 mAg^{-1}.[12] However, the low mass ratio of P-Si (50 wt%) affects the power density and energy density for practical application. Since the lithiation/delithiation process only takes place in the surface layer of Si particles, a large portion of the active materials is not utilized for micro-sized particles. The development of nano-sized Si particles with a higher specific area is desired for the lithiation process.

Despite the recognition of heteroatom doping effect on improving the electrochemical performance of Si, there have been no studies of how nanoscale size and the ppm-level surface layer P-doping affect the battery performance. We hypothesized that the nano-sized P-Si could enable high columbic efficiency and shorten lithium ion and electron transport pathways. The ppm-level introduction of P atoms leads to a small increase of the lithium insertion energy while maintaining the activity and conductivity of Si nanomaterials. Besides, by employing graphene as buffer matrix and conductive network, the P-Si/G nanocomposite is expected to further enhance the cycling stability and high rate capability. To demonstrate the feasibility, we synthesized graphene-wrapped, nano-sized P-Si via a chemical reduction method. This report describes the new findings of our investigation of the P-Si/G nanocomposite to demonstrate the viability of enhancing the cycling stability and rate capability of Si-based anode materials. The structural integrity and stability was further improved by coupling with electrostatic and hydrogen-bonding interactions of a bio-degraded poly-γ-glutamate binder, leading to a unique self-healing capability. The understanding of the role of the electrostatic and hydrogen-bonding interactions in the self-

[a] *Department of Chemistry, State University of New York at Binghamton, Binghamton, New York 13902, United States*
[b] *School of Chemical Engineering and Technology, Tianjin University, Tianjin, 300350, China*
[c] *Suzhou Gorichen Technology Co., Suzhou Wuzhong Economic Development Zone, China*
Electronic Supplementary Information (ESI) available:

healing mechanism is the focus of our investigation describved in this report.

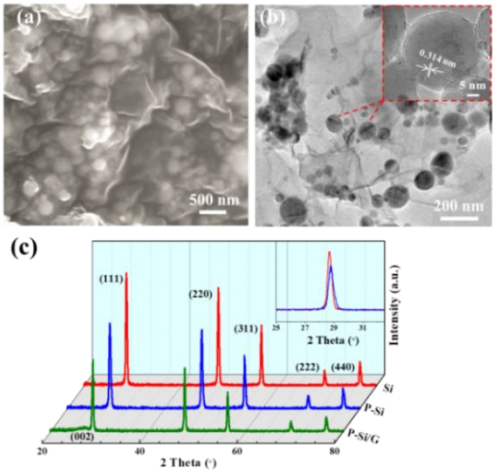

Fig.1 (a-b) SEM (a) and TEM images (b) of P-Si/G nanocomposite; (c) XRD patterns of Si powder, P-Si nanoparticles, and P-Si/G nanocomposite.

Figure 1a shows a representative SEM image of P-Si/G. It can be seen that the graphene sheets form a consecutive network by interconnection among the different sheets. The P-Si nanoparticles with an average diameter of 110 nm are embedded inside the network. This conductive network could provide an additional electron transfer pathway which is expected to further enhance the conductivity of P-Si. The TEM image in **Figure 1b** provides some structural details of the P-Si/G composite. The P-Si nanoparticles are dispersed well in the wrinkled graphene thin layer. The lattice fringe, 0.314 nm, as shown in inset **Figure 1b**, is consistent with the (111) plane of the crystalline silicon. Both P-Si and graphene appear to be well mixed. The graphene thin layer outside P-Si nanoparticles could prevent the side reaction of P-Si with electrolyte to occur. In **Figure 1c**, the XRD patterns of Si powder, P-Si nanoparticles and P-Si/G are compared. All the peaks are in good agreement with Si (JCPDS No. 77-2108). A diffraction peak appears around 26° is attributed to the (002) plane of graphene. Peaks observed at 28.5°, 47.4° and 56.2° exist in all the three samples correspond to the (111), (220) and (311) plane of Si. In the magnified XRD patterns of Si and P-Si, it can be observed that the intensity of P-Si is lower than pristine Si and the XRD peak of Si (111) shifts slightly to higher angle after introducing P. This is because some of the Si atoms are replaced by P atoms and no other peaks can be observed from the XRD pattern, implying there exists less impurities in all the three samples.[11]

The content of graphene in as-obtained P-Si/G is evaluated by TGA (**Figure S1**). The main mass loss is shown to happen below 650 °C, which is ascribed to the combustion of graphene. The overall content of graphene is 14.5 wt% in P-Si/G. The mass displays a continuous increase after 650 °C, which is ascribed to the oxidation of Si.[13]

Figure 2 displays a representative set of CV curves of the P-Si/G electrode for the initial 5 cycles in the voltage range of 0.05 - 1 V *vs*. Li^+/Li at a sweep scan rate of 0.1 mV s^{-1}. The current can only be observed until 0.09 V on the first cathodic scan. The lower potential is related to the smaller thermodynamic driving force for lithiation.[14] The cathodic peak at 0.2 V shown in the following cycles is ascribed to the lithiation of amorphous Si. In the anodic scan, two distinct peaks shown at 0.41 V and 0.56 V are related to the delithiation process of Li_xSi.[15] It is worth noticing that the current shown in the CV curves increases with the scanning time. This reflects the activation process of Si at the initial stage, which is consistent with previous report.[16] The galvanostatic discharge/charge profiles of P-Si/G electrode are examined, as shown in **Figure S2** for the initial five cycles. In the first discharge curve, the plateau appears 0.09 V corresponds to lithiation of crystalline Si which is in agreement with the CV result. The initial discharge and charge capacity of P-Si/G are 3,592 mA h g^{-1} and 2,938 mA h g^{-1}. The large capacity loss is attributed to the formation of SEI and side reaction of graphene. It can be observed that the curves begin to overlap after the 2nd cycle, indicating that the electrode structure is relatively stable.

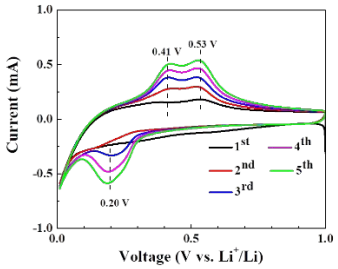

Figure 2. Cyclic voltammetric curves showing the electrochemical performance of the P-Si/G composite.

To evaluate the cycling performance of P-Si/G electrode, galvanostatic charge/discharge tests were carried out at 400 mA g^{-1} and the results are shown in **Figure 3a**. Distinct capacity decay was observed only in the initial 10 cycles with initial coulombic efficiency of 81.9%. In the following cycles, a reversible capacity of 1413.5 mA h g^{-1} retains after 100 cycles. In comparison, P-Si, Si, P-Si/CNT and P-Si/GNPs electrodes were tested under the same condition with a reversible capacity of 512.9, 481.5, 545.8 and 632.9 mA h g^{-1} after 100 cycles as shown in **Fig. S3**. The corresponding initial coulombic efficiency is shown in inset of **Fig. S3**, they are 81.4%, 72.3%, 80.7% and 78.5%, which are lower than P-Si/G electrode. Even though combining carbon materials with P-Si can improve the conductivity and the capacity retention is improved to some extent, a simple mixing of carbon (same amount with graphene) with P-Si cannot ensure that P-Si nanoparticles are fully wrapped with carbon. As such, the exposure of a large amount of unwrapped P-Si to the electrolyte would lead to the capacity decay due to unstable SEI caused by volume effect.

The surface morphologies of the cycled Si and P-Si/G electrodes were characterized by SEM, as shown in **Figure S4**. It is clearly seen that there exists many cracks on the surface of Si electrode. The surface of P-Si/G electrode is smooth and uniform, indicating the electrode structure is stable. Compared with the other three Si/C composites electrodes, the outstanding cycling performance of P-Si/G electrode can be attributed to the presence of flexible graphene protective layer outside P-Si nanoparticles. The P-Si nanoparticles embedded in the voids in

the graphene layers which provide enough space for the volume expansion during the lithiation/delithiation process. As a result, the structural stability of electrode would be enhanced. Meanwhile, most of the P-Si nanoparticles are wrapped by the graphene. This would largely avoid the active material from directly contacting with electrolyte and build a stable SEI. Therefore, the coulombic efficiency is improved. Moreover, the cross-linked, wrinkled graphene with a few layers serves as a good conductive network compared with multi-layered GNPs since there is less resistance for charge transfer.

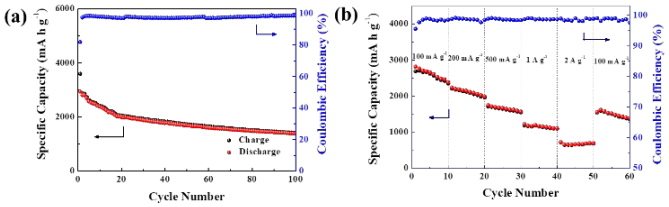

Figure 3. Cycling performance of P-Si/G electrode: (a) Capacity at current density of 400 mA g^{-1}; and (b) rate capability.

Rate capability of P-Si/G electrode was determined under different current densities from 100 mA g^{-1} to 2 A g^{-1} for 10 cycles at each current density. A representative set of the data is shown in **Figure 3b**. From lower to higher current density, the reversible capacity showed gradual and small drops but relatively stable. The corresponding reversible capacity of P-Si/G tested at 100, 200, 500, 1,000 and 2,000 mA $g^{-1}$are 2,400, 1,992, 1,568, 1,133 and 672 mA h g^{-1}. Remarkably, when returning to 100 mA g^{-1}, the capacity can still reach to 1,386 mA h g^{-1}, indicating that the structure of P-Si/G electrode is relatively stable.

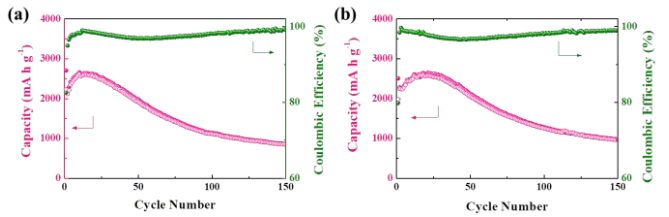

Figure 4. Cycling performance of P-Si/G nanocomposite electrode with different binder modifications: (a) PGA; and (b) ammonium modified PGA (testing under 1A g^{-1} for 150 cycles).

For Si nanoparticles electrode, the cycling performance showed a significant improvement when utilizing polyglutamic acid (PGA) as binder, compared with commercial PVDF and sodium alginate (as shown in **Figure S5**). A high rate performance of Si electrode was obtained when PGA was modified by ammonium, in comparison with PGA modified by other cations (e.g. Li^+, Na^+, K^+, see **Figure S6**). It is an excellent binder for Si electrode as evidenced by the good cycling performance of P-Si/C at low current density. We expect that a further enhancement of the high rate capability is possible by optimizing the composition of PGA in the nanocomposite which contributes to the cycling stability. The performances of the electrodes derived from using PGA and ammonium modified PGA as binders were compared under the same current density of 1 A g^{-1}. The results for 150 cycles are shown in **Figure 4**. The reversible capacity of the P-Si/G electrode showed an increase during the first 10 cycles, which could be attributed to activation of the nanomaterials as supported by earlier findings [17]. A reversible capacity of 894 mA h g^{-1} was retained for the electrode with PGA after 150 cycles. The cycling performance was shown to further increase, displaying a reversible capacity of 1002 mA h g^{-1} for the electrode derived utilizing ammonium modified PGA under the same testing condition. The coulombic efficiency under high current density is slightly lower than the one tested under lower current density due to a larger volume expansion in a short time. As shown in Table S2 comparing the mass loading and electrochemical performance of previous reports on Si-based anode, the cycling performance and rate capability of our P-Si/G electrode are clearly improved to a great extent over the existing materials. To test the potential application as the anode material for lithium-ion battery, we assembled a full cell using the P-Si/G as the anode and lithium cobalt oxide as the cathode. Part of the future work involves full cell testing with other different reference samples. A good cycling performance was observed in the voltage window of 2.0 - 4.3 V at a current density of 100 mA g^{-1} (**Figure S7**). Further support for the self-healing capability is provided by the result from analysis of the morphological evolution of the P-Si/G electrode with ammonium modified PGA as binder immediately after 1 cycle and 5 min rest time following the cycle (**Figure S8**). The result revealed a clear reduction of cracks in the nanocomposite film on the electrode as a function of time.

In the polymeric structure, there is a significant role in the stability being played by the combination of electrostatic-binding and hydrogen-binding between adjacent carboxylic acid, ammonium, and carboxylate groups. The polymeric and hydrogen-bonding structures enable maneuvering of the mechanical stress caused by the reaction-induced volume expansion. The close contact of the polymeric structure with the conductive materials and current collector is hypothesized to facilitate the self-healing possess. To test this hypothesis, we compared the electrochemical impedance spectra (EIS) of P-Si/G electrodes derived from utilizing PGA and sodium alginate as a binder. The experiment was carried out in the range of 100 kHz to 10 mHz after the 1st discharge to 0.05 V and being held for different times (Figure S9a and b). By analyzing the data in terms of the equivalent circuit, the spectra can be divided into three parts: two depressed semicircles in the high frequency region and a sloped line in the low frequency region. The depressed semicircle in the high frequency region corresponds to the interface resistance (R_S) which is related to the resistance of the SEI film and the charge/discharge resistance of lithium-ion insertion (R_{ct}).[18] It is noteworthy that all the spectra are not overlapped as the standing time prolongs. The EIS data were analyzed by model fitting, and the changes of R_{ct} and R_s values over time were compared (Figure S9c and d). For the nanocomposite electrode using sodium alginate as a binder, both R_{ct} and R_s are shown to increase continuously after discharge, which is indicative of the continuous cracking of the active materials. This trend lasted for 90 min before reaching a plateau. For the nanocomposite electrode using PGA as a binder, R_{ct} and R_s show a decrease to a stable value in the first

60 min. Based on the trend of R_{ct} and R_s vs. time, it takes shorter time for electrode using PGA as binder. The decreased R_{ct} and R_s values in the case of PGA demonstrates that the integrity of the nanocomposite is largely maintained as a result of the self-healing capability during the cycling process, which is facilitated by the flexibility of PGA polymer in the nanocomposite structure.

Figure 5a descripts charge/discharge process in the network structure of P-Si/G-PGA electrode. The volume expansion degree of Si crystal is limited to some extend due to the shrinkage of P-Si crystal. Meantime, the PGA and ammonium modified PGA involving hydrogen bonding (I), electrostatic bonding (II), and combination of hydrogen bonding and electrostatic bonding (III). The prominent cycling capability is attributed to the flexibility of hydrogen bonded polymeric network.

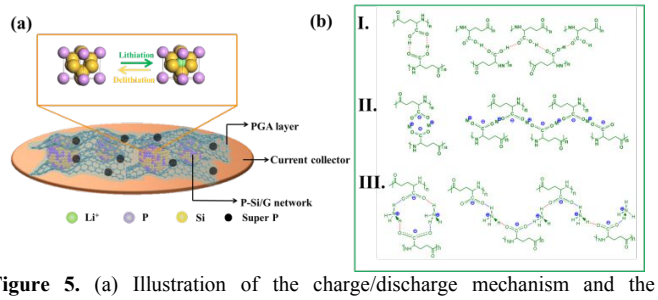

Figure 5. (a) Illustration of the charge/discharge mechanism and the conductive and stress-buffering network of P-Si/G-PGA; and (b) Schematic illustration of the interactions in the network involving hydrogen bonding (I), electrostatic bonding (II), and combination of hydrogen bonding and electrostatic bonding (III).

For PGA, there exist two types of hydrogen bonding for the carboxylic acid groups: "head-to-head" and "shoulder-to-shoulder" hydrogen bonding. In the case of ammonium modified PGA, there is a combination of electrostatic interaction and hydrogen bonding among the NH_4^+ and $-CO_2^-$ groups. This type of intermolecular interactions poses a strong binding capability which facilitates the maintenance of the integrity of electrode after cycles. This assessment is supported by FTIR spectra of the PGA and the ammonium modified PGA (Figure S10). For PGA, the peak observed around 1720 cm^{-1} is ascribed to –COOH groups in dimetric hydrogen bonding mode. The peak shwon around 1625 cm^{-1} corresponds to those in polymetric hydrogen bonding mode. For the ammonium modified PGA, the 1720 cm^{-1} disappears and a broad peak is shown at ~1550 cm^{-1} which corresponds to the $-CO_2^-$ group[19]. When the PGA is modified by ammonium, there is polyanionic structure interacting with NH_4^+ ions. The electrostatic attraction is much stronger than the hydrogen bonding, which is believed to have played an important role in enabling the ammonium modified PGA with a higher efficiency for improving the close contact with active materials, thus contributing to a better self-healing capability for enhancing the electrode stability. As shown Fig. S11 by comparing the overall morphologies of P-Si/G electrodes after 100 cycles for materials with sodium alginate, PGA and ammonium modified PGA as binders, there exists a problem of peeling off for the electrode materials using sodium alginate as binder. In contrast, the electrode materials with PGA and ammonium modified PGA displays much better maintenance of the overall morphology as a result of the unique intermolecular interaction.

In summary, we have for the first time successfully designed nanocomposite anode materials consisting of ppm-level phosphorus-doped Si nanoparticles (P-Si) wrapped in a network of poly-γ-glutamate and graphene. The great improvement in electrochemical performance of this nanocomposite anode combines the structural stability of the nano structure and extraordinary binding capability of poly-γ-glutamate originates from the combination of electrostatic interaction and hydrogen bonding as the intermolecular interaction in the nanocomposite structure. These findings should have immediate implications to the design of high-performance Si nanomaterials for use as anode materials in lithium ion batteries.

This work was financially supported by the National Science Foundation (CHE 1566283, IIP 1640669). RN also acknowledges the support from China Scholarship Council.

Conflicts of interest

There are no conflicts to declare.

References

1. G. Armstrong, *Nature chemistry*, 2019, **11**, 1076.
2. Y. Lu, L. Yu and X. W. Lou, *Chem*, 2018, **4**, 972-996.
3. X. Zhang, D. Kong, X. Li and L. Zhi, *Advanced Functional Materials*, 2019, **29**, 1806061.
4. L. Zhao, J. C. Bennett, A. George and M. N. Obrovac, *Chemistry of Materials*, 2019, **31**, 3883-3890.
5. Y. Lin, Y. Chen, Y. Zhang, J. Jiang, Y. He, Y. Lei, N. Du and D. Yang, *Chemical Communications*, 2018, **54**, 9466-9469.
6. L. Zhang, K. Zhao, R. Yu, M. Yan, W. Xu, Y. Dong, W. Ren, X. Xu, C. Tang and L. Mai, *Small*, 2017, **13**.
7. C.Y. Jung, J.B. Koo, B.Y. Jang, J.S. Kim, J.S. Lee, S.S. Kim and M.H. Han, *Thin Solid Films*, 2015, **587**, 142-149.
8. M. Chen, B. Li, X. Liu, L. Zhou, L. Yao, J. Zai, X. Qian and X. Yu, *Journal of Materials Chemistry A*, 2018, **6**, 3022-3027.
9. B. R. Long, M. K. Y. Chan, J. P. Greeley and A. A. Gewirth, *The Journal of Physical Chemistry C*, 2011, **115**, 18916-18921.
10. M. Ge, J. Rong, X. Fang and C. Zhou, *Nano letters*, 2012, **12**, 2318-2323.
11. Y. Domi, H. Usui, M. Shimizu, Y. Kakimoto and H. Sakaguchi, *ACS Applied Materials & Interfaces*, 2016, **8**, 7125-7132.
12. S. Huang, L. Z. Cheong, D. Wang and C. Shen, *ACS Applied Materials & Interfaces*, 2017, **9**, 23672-23678.
13. X. Cheng, R. Na, X. Wang, N. Xia, Z. Shan and J. Tian, *Inorganic Chemistry Frontiers*, 2019, DOI: 10.1039/c9qi00488b.
14. C. Yan, Q. Liu, J. Gao, Z. Yang and D. He, *Beilstein Journal of Nanotechnology*, 2017, **8**, 222-228.
15. M. T. McDowell, S. W. Lee, W. D. Nix and Y. Cui, *Advanced Materials*, 2013, **25**, 4966-4985.
16. M.J. Choi, Y. Xiao, J.Y. Hwang, I. Belharouak and Y.K. Sun, *Journal of Power Sources*, 2017, **348**, 302-310.
17. Z.W. Lu, G. Wang, X. P. Gao, X. J. Liu and J. Q. Wang, *Journal of Power Sources*, 2009, **189**, 832-836.
18. R. Malik, M. J. Loveridge, L. J. Williams, Q. Huang, G. West, P. R. Shearing, R. Bhagat and R. I. Walton, *Chemistry of Materials*, 2019, **31**, 4156-4165.
19. W. Zheng, M.M Maye F.L. Leibowitz, and C.J. Zhong, *Analytical Chemistry*, 2000, **72**, 10.

Table of contents entry

A network of graphene conductive stress buffer and poly-γ-glutamate binder via interparticle electrostatic and hydrogen bonding is constructed for the improved multifunctional Si nanocomposite anode of lithium-ion battery.